Journal of Inorganic Biochemistry 116 (2012) 151–162

Contents lists available at SciVerse ScienceDirect

Journal of Inorganic Biochemistry

journal homepage: www.elsevier.com/locate/jinorgbio

New $[Ru(5,6\text{-dmp}/3,4,7,8\text{-tmp})_2(diimine)]^{2+}$ complexes: Non-covalent DNA and protein binding, anticancer activity and fluorescent probes for nuclear and protein components

Venugopal Rajendiran [a,1], Mallayan Palaniandavar [a,*], Vaiyapuri Subbarayan Periasamy [b], Mohammad Abdulkader Akbarsha [b]

[a] School of Chemistry, Bharathidasan University, Tiruchirapalli 620 024, India
[b] Department of Animal Science, Bharathidasan University, Tiruchirapalli 620 024, India

ARTICLE INFO

Article history:
Received 8 January 2012
Received in revised form 2 June 2012
Accepted 4 June 2012
Available online 18 June 2012

Keywords:
Ru (II) polypyridyl complexes
DNA binding
Protein binding
Anticancer activity
Nuclear staining agent
Protein staining agent

ABSTRACT

A series of Ru(II) complexes of the type $[Ru(5,6\text{-dmp})_2(diimine)]^{2+}$ **1–3** and $[Ru(tmp)_2(diimine)]^{2+}$ **4–6**, where 5,6-dmp is 5,6-dimethyl-1,10-phenanthroline, tmp is 3,4,7,8-tetramethyl-1,10-phenanthroline and diimine is dipyrido-[3,2-*d*:2′,3′-*f*]-quinoxaline (dpq), dipyrido[3,2-*a*:2′,3′-*c*]phenazine (dppz) and 11,12-dimethyl-dipyrido[3,2-*a*:2′,3′-*c*]phenazine (11,12-dmdppz), has been isolated and the DNA binding mode of the complexes studied by using emission and circular dichroic (CD) spectral techniques. All the complexes exhibit induced circular dichroism upon binding to calf thymus (CT) DNA and show preferential binding to AT and mixed $(d(CGCGATCGCG)_2)$ sequences rather than to GC sequences. The complex $[Ru(tmp)_2(dpq)]^{2+}$ **4** exhibits enhancement in luminescence higher than $[Ru(5,6\text{-dmp})_2(dpq)]^{2+}$ **1** upon binding to DNA. In contrast, $[Ru(5,6\text{-dmp})_2(dppz)]^{2+}$ **2** and $[Ru(5,6\text{-dmp})_2(dmdppz)]^{2+}$ **3** exhibit luminescence enhancement higher than $[Ru(tmp)_2(dppz)]^{2+}$ **5** and $[Ru(tmp)_2(dmdppz)]^{2+}$ **6** respectively upon DNA binding, illustrating the importance of hydrophobic forces of interaction in determining the DNA binding affinity. Among the complexes, **4** exhibits the highest enhancement in fluorescence intensity upon binding to the protein bovine serum albumin (BSA). The cytotoxicity of the complexes has been studied by screening them against non-small lung carcinoma (NCI-H460) cell line. It is noteworthy that the complex showing the strongest DNA binding affinity exhibits the highest cytotoxicity. The efficiency of the complexes as fluorescent probes for detection of nuclear morphology and proteins has been evaluated by using fluorescence microscopy. Remarkably, **4**, which shows strong hydrophobic forces of interaction when bound to DNA and protein, acts as fluorescent probes for detection of nuclear components in the head, and proteins in the tail, of sperms.

1. Introduction

Coordination complexes of Ru(II) with polyazaheterocyclic chelating ligands have found widespread application as protein markers in hydrodynamic and photoinduced electron-transfer studies [1–5], as molecular probes of DNA [6,7] and as stains for both isolated DNA and that in fixed cell nuclei [8]. The most interesting complexes investigated so far are $[Ru(bpy)_2(dppz)]^{2+}$ (bpy = 2,2′-bipyridine) [9] and $[Ru(phen)_2(dppz)]^{2+}$ (phen = 1,10-phenanthroline) [10], both containing the intercalating ligand dipyrido[3,2-a:2′,3′-c]phenazine (dppz). They bind to DNA with the highest affinity ($K_b > 10^6\ M^{-1}$) [9,10] and, interestingly, although lacking luminescence in aqueous solution, they show intense luminescence (molecular light switch effect) in the presence of double helical DNA, a property that makes them interesting as DNA stains. Also, a series of $[Ru(phen)_2(L)]^{2+}$ complexes, where L is a substituted dppz ligand, have been investigated as luminescence reporters of DNA [11]. Very recently, Barton and her co-worker [12] have explored the cellular uptake of Ru(II) complexes and found that the complex cation $[Ru(dip)_2(dppz)]^{2+}$ (dip = 4,7-diphenyl-1,10-phenanthroline) is effectively transported into the cellular interior. These complexes have been exploited as probes to examine the local structural polymorphism of nucleic acids, as photo reactive reagents targeted to recognize mismatches or to repair thymine dimers and as probes of long range charge transport through the DNA helix [13–18]. Also, the DNA bisintercalator complex Δ–Δ[μ-C4(cpdppz)$(phen)_4Ru_2]^{4+}$, where C4(cpdppz) = *N*,*N*′ bis(cpdppz)-1,4-diaminobutane; cpdppz = 12-cyano-12,13-dihydro-11 *H*-cyclopenta[b] dipyrido[3,2-*h*:2′3′-*j*]phenazine-12-carbonyl, acts as a DNA staining agent for V79 Chinese hamster cells [19,20].

* Corresponding author at: Department of Chemistry, School of Basic and Applied Sciences, Central University of Tamil Nadu, Thiruvarur 610 004, India. Fax: +91 4312407043.
E-mail addresses: palanim51@yahoo.com, palaniandavarm@gmail.com (M. Palaniandavar).
[1] Present address: Department of Chemistry, School of Basic and Applied Sciences, Central University of Tamil Nadu, Thiruvarur 610 004, India.

0162-0134/$ – see front matter © 2012 Elsevier Inc. All rights reserved.
doi:10.1016/j.jinorgbio.2012.06.005

Since the metal-to-ligand charge transfer transition (MLCT) in $[Ru(bpy)_2(dppz)]^{2+}$ is located on the dppz ligand involved in intercalative DNA interaction leading to luminescence enhancement, substitution has been made in the diimine ligands in $[Ru(diimine)_2(dppz)]^{2+}$ to tune the redox, optical and DNA-binding properties of the complexes [21–23]. An increase in surface area of the primary ligand as in $[Ru(ip)_2(dppz)]^{2+}$, where ip = imidazo[4,5-*f*][1,10]-phenanthroline, enhances the DNA binding affinity of the complex [24,25]. We have very recently shown that the 5,6-dmp ligand in *rac*-$[Ru(5,6\text{-}dmp)_2(dppz)]^{2+}$ strongly favors the formation of a stable structural and electronic scaffold on the DNA surface for the unbound molecules to couple with the DNA-bound complexes facilitating spontaneous assembly of novel extended molecular aggregates [26]. Gyarfas and his co-workers have reported that $[Ru(tmp)_3]^{2+}$, where tmp is 3,4,7,8-tetramethyl-1,10-phenanthroline, exhibits tumor inhibiting properties [27]. Kruger and his co-workers [28] have reported that Ru(II) complexes of some of the methyl substituted derivatives of dpq exhibit unusual photophysical switching upon binding to DNA.

Like DNA, protein is also considered to be one of the prime molecular targets for diagnostic and imaging agents, and so equal attention has been paid on designing novel probes for proteins [29–31]. Certain platinum containing compounds have been reported as molecular light-switches for proteins [32]. Very recently, we have demonstrated that the complex $[Cu(tdp)(tmp)]^{+}$ (tmp = 3,4,7,8-tetramethyl-1,10-phenanthroline), which binds to proteins more strongly and exhibits cytotoxicity higher than the analogous complexes [33].

In this study we have prepared a series of Ru(II) complexes of the type $[Ru(5,6\text{-}dmp)_2(diimine)]^{2+}$ **1**–**3** and $[Ru(tmp)_2(diimine)]^{2+}$ **4**–**6**, where diimine is an extended ligand (Scheme 1) such as dipyrido-[3,2-*d*:2′,3′-*f*]-quinoxaline (dpq), dppz and 11,12-dimethyldipyrido [3,2-a:2′,3′-c]phenazine (11,12-dmdppz) on the optical, electrochemical and DNA and protein binding properties of the complexes. We have incorporated methyl substitution on positions 11 and 12 of the phenazine part of dppz (11,12-dmdppz) because Lincoln and his co-workers have found that incorporation of 11,12-dmdppz or 10-mdppz (10-mdppz = 11-methyldipyrido[3,2-a:2′,3′-c]phenazine in Ru(II) complexes causes an increase in the excited state lifetime upon binding to CT DNA [34]. The DNA and protein binding of the present Ru(II) complexes has been studied by using a variety of physical methods like emission and circular dichroic spectroscopy, and attempts are made to exploit the new mixed ligand complexes $[Ru(5,6\text{-}dmp/tmp)_2(diimine)]^{2+}$ as fluorescent DNA and protein probes. It is noteworthy that the complex $[Ru(tmp)_2(dpq)]^{2+}$ **4** acts as a fluorescent probe for detection of cell morphologies in tissue section, DNA and proteins in the sperm head and tail respectively by using fluorescent microscopy. Also, the cytotoxicity of the complexes has been studied by screening them against non-small lung carcinoma (NCI-H460) cell line, and it depends upon both the primary and secondary ligands.

2. Results and discussion

2.1. Synthesis and characterisation of Ruthenium(II) complexes

The mixed ligand complexes $[Ru(5,6\text{-}dmp)_2(diimine)](PF_6)_2$ **1**–**3** and $[Ru(tmp)_2(diimine)](PF_6)_2$ **4**–**6** have been isolated by reacting the complexes $[Ru(5,6\text{-}dmp)_2Cl_2]Cl$ and $[Ru(3,4,7,8\text{-}tmp)_2Cl_2]Cl$ with the corresponding diimine ligands. The CHN analyses of the complexes are consistent with the formula $[Ru(5,6\text{-}dmp/tmp)_2(diimine)](PF_6)_2$, which is supported by ESI-MS analysis. The NMR spectra show that the ligands are bound to Ru(II). The PF_6 salts of the complexes are soluble in polar solvents like acetonitrile, DMF and DMSO etc but not in water and ether. The chloride salts of **1**, **2**, **4** and **5** are highly soluble in water but those of **3** and **6** are soluble in 5% DMF/5 mM Tris–HCl/50 mM NaCl buffer at pH 7.1. So the experimental solutions of all the complexes were prepared in 5% DMF/5 mM Tris–HCl/50 mM NaCl buffer at pH 7.1 and 5% DMF/NaH_2PO_4:$NaHPO_4$ buffer at pH 7.1for DNA and protein binding studies respectively. For cytotoxic studies we have used 1% DMSO buffer solution as we found that 1% DMSO buffer is non-toxic to cells. The stability of the complexes in DMF and DMSO buffers has been checked by using the UV–visible (UV–VIS) spectral features of the solutions. Even after two weeks

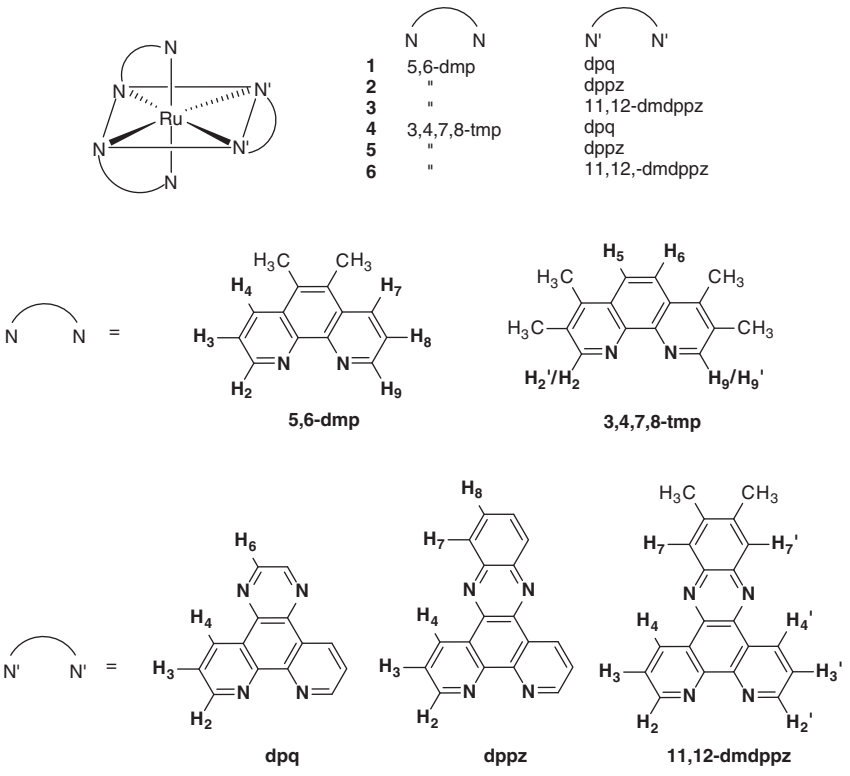

Scheme 1. Structures of Ru(II) complexes and diimine ligands.

time we found that the spectral characteristics did not change, revealing that the compounds are stable enough in both the buffers.

2.2. Electronic absorption spectral and redox properties

In 5% DMF/5 mM Tris–HCl/50 mM NaCl buffer at pH 7.1 all the complexes display a high energy intra-ligand π–π* band (234–386 nm, Table 1) [35] and the MLCT bands (420–475 nm, Table 1), which are typical of Ru(II) complexes with coordinated polyimine ligands [12]. The MLCT band energies (420–424 nm) of the tmp complexes **4**–**6** are higher than those for the 5,6-dmp complexes **1**–**3** (445–453 nm), possibly because the incorporation of four electron-releasing methyl groups to obtain **4**–**6** enhances the electron density on Ru(II), leading to the raise in energy of Ru(II) dπ orbitals and hence the observation of the MLCT band involving the co-ligands at lower energy.

In acetonitrile solution all the complexes exhibit a quasi-reversible (ΔE_p, 80–104 mV) metal-based oxidative response (Fig. 1, Table 2) with $E_{1/2}$ values falling in the range of 0.869–1.029 V. The Ru(II)/Ru(III) redox potentials of the 5,6-dmp complexes **1**–**3** are more positive than those of the corresponding tmp complexes **4**–**6**. This trend is consistent with the lower MLCT band energies of the 5,6-dmp complexes **1**–**3** (cf. above). The number of electron-releasing methyl groups in **4**–**6** is higher than those in **1**–**3** leading to destabilize the Ru(II) oxidation state and hence the lower Ru(II)/Ru(III) redox potential of the former complexes. Also, the Ru(II)/Ru(III) redox potential becomes more positive as the dpq ligand in **1** and **4** is replaced by the dppz ligand with enhanced π-delocalization to obtain **2** and **5** respectively, revealing stabilization of Ru(II) oxidation state in the latter complexes. Further, the Ru(II)/Ru(III) redox potentials of **3** and **6** are less positive than those of **2** and **5** respectively, which is due to the increase in the electron density upon leading to destabilization of Ru(II) oxidation state (cf. above). All the complexes display two irreversible reduction waves in the potential range of −1.191 to −1.852 V, which arise from the addition of electrons into the electrochemically accessible LUMO [36,37] of the more π-delocalized co-ligands.

2.3. DNA binding studies

2.3.1. Steady-state emission studies

All the present Ru(II) complexes luminesce in aqueous solution (5% DMF/5 mM Tris–HCl/50 mM NaCl buffer at pH 7.1) upon irradiation in the MLCT band. No attempt was made to eliminate oxygen from solutions used in the emission experiments since the focus of the present study is on assessing the utility of the complexes as probes for DNA. The emission maxima vary, as do the intensities, but fall within the narrow range of 586–614 nm. The luminescence observed for the present complexes is relatively low in aqueous solution but is enhanced in the presence of calf thymus (CT) DNA (Fig. 2, Table 3). The observed enhancement is similar to that for the so-called [38] 'molecular light-switches' such as $[Ru(bpy)_2(dppz)]^{2+}$ and $[Ru(phen)_2(dppz)]^{2+}$ and the quinoxaline (**1**) and phenazine (**2**) nitrogen atoms of DNA-intercalated excited state complexes are well protected from access by water molecules leading to the observed emission enhancement. The relative emission intensity (I/I_0) versus R (=[DNA]/[Ru(II) complex]) plot (Fig. 3) reveals that the luminescence enhancement for the 5,6-dmp complexes varies as **1**<**2**>**3** and that for the tmp complexes varies as **4**>**5**<**6** (cf. below).

The steady-state luminescence titration data have been analyzed by using Mc Ghee von Hippel equation [39] for non-co-operative binding model by non-linear least-squares analysis. A known amount (10 μM) of **1**–**6** was titrated with DNA over a range of the DNA concentration (5.0×10^{-6}–4.0×10^{-4} M, R = 0–40 = [DNA]/[Ru(II) Complex]). The concentration of the bound Ru(II) complex was calculated using Eq. (1):

$$c_b = c[(I-I_0)/(I_{max}-I_0)] \quad (1)$$

where c is the total Ru(II) complex concentration, I and I_0 are the emission intensities in the presence and absence of DNA, and I_{max} is the fluorescence of the totally bound complex. The concentration of the free complex, c_f, is equal to $(c-c_b)$. A plot of r/c_f vs r, where r is c_b/[DNA], was constructed according to the Mc Ghee von Hippel equation:

$$2r/c_f = K_b(1-2nr)[(1-2nr)/\{1-2(n-1)r\}](n-1) \quad (2)$$

where K_b represents the intrinsic binding constant of the complexes with DNA and n is the size of a binding site in base pairs. The binding data were fitted (Figs. 4 and 5) to Eq. (2), and the observed intrinsic binding constants (K_b, $0.03–4.0\times10^7$ M^{-1}) along with the DNA binding site sizes (n, 6–10.5 base pairs), are collected in Table 3. The values of K_b are comparable to that of the known intercalator $[Ru(bpy)_2(phi)]Cl_2$ [24]. The binding site sizes are comparable to those of the well-known partially intercalating Ru(II) polypyridine complexes such as $[Ru(bpy)_2(phen)]^{2+}$, $[Ru(phen)_3]^{2+}$ and $[Ru(phen)_2(flone)]^{2+}$ [40] (flone = 4,5-diazafluorene-9-one). Among the 5,6-dmp complexes the value of K_b varies as **1**<**2**>**3**, which is in line with the observed enhancement in emission (cf. above). Thus **2** exhibits DNA binding affinity higher than **1** because the coordinated dppz of **2** is inserted into the DNA base pairs much deeper than the dpq of **1**, leading to higher stabilization of the excited state and hence higher enhancement in emission (cf. above). The methyl groups in dmdppz (**3**) prevents the partial intercalation of **3** into DNA and so DNA groove binding is preferred for **3**, leading to weaker DNA binding of the complex. Also, the MLCT excited state localized on dmdppz ligand of **3** is less well preserved from access by water molecules and hence the 'molecular light switch' effect of **3** is less than that of its dppz analogue **2** (cf. above). In contrast to the 5,6-dmp complexes, the DNA binding affinity of the tmp complexes

Table 1
Absorption spectral properties of Ru(II) complexes[a].

Complex	λ/nm (ε/M^{-1} cm^{-1})
$[Ru(5,6\text{-dmp})_2(dpq)]^{2+}$ **1**	448 (12 250), 425 (sh) (11 650), 296 (sh) (28 136), 267 (34 540)
$[Ru(5,6\text{-dmp})_2(dppz)]^{2+}$ **2**	445 (17 820), 374 (19 090), 270 (32 660), 240 (59 840)
$[Ru(5,6\text{-dmp})_2(dmdppz)]^{2+}$ **3**	453 (14,730), 383 (32,580), 275 (47,300)
$[Ru(3,4,7,8\text{-tmp})_2(dpq)]^{2+}$ **4**	475 (sh) (8120), 421 (17,020), 302 (sh) (27,720), 266 (89,420)
$[Ru(3,4,7,8\text{-tmp})_2(dppz)]^{2+}$ **5**	424 (13,910), 376 (13,150), 360 (11,390), 272 (66,640), 234 (39,720)
$[Ru(3,4,7,8\text{-tmp})_2(dmdppz)]^{2+}$ **6**	420 (7190), 386 (8400), 268 (21,630)

[a] Measured in 5% DMF/5 mM Tris–HCl/50 mM NaCl buffer at pH 7.1.

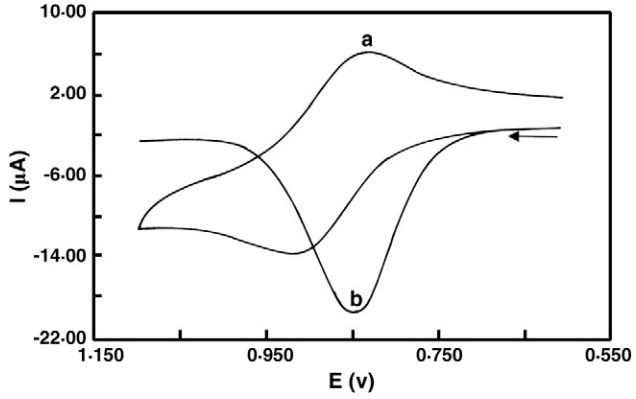

Fig. 1. (a) Cyclic and (b) differential pulse voltammograms of 0.25 mM complex $[Ru(tmp)_2(dppz)]^{2+}$ **5** in acetonitrile solution at 25.0 ± 0.2 °C at 0.05 Vs^{-1} scan rate.

Table 2
Redox properties of Ru(II) complexes[a,b,c] at 25.0 ± 0.2 °C.

Compound	E_{pa} V	E_{pc} V	ΔE_p mV	$E_{1/2}$[d] V	$E_{1/2}$[e] V	$D\times10^6$ $cm^2\ s^{-1}$
1	1.004	0.904	100	0.954	0.945	10.7
				−1.341		
				−1.830		
2	1.314	1.056	105	1.185	1.189	1.8
				−1.240		
				−1.940		
3	1.082	0.978	104	1.030	1.029	9.5
				−1.238		
				−1.852		
4	0.934	0.842	92	0.888	0.875	7.2
				−1.288		
				−1.790		
5	0.920	0.840	80	0.880	0.877	8.2
				−1.214		
				−1.809		
6	0.914	0.826	88	0.870	0.869	7.9
				−1.191		
				−1.464		

[a] Measured *vs* non-aqueous Ag/Ag^+ reference electrode; add 544 mV [300 mV, Ag/Ag^+ to SCE + 244 mV, SCE to SHE] to convert to standard hydrogen electrode (SHE); scan rate, 50 mV s^{-1}; supporting electrolyte, $[(C_4H_9)_4N](ClO_4)$ (0.025 M).
[b] Complexes **1**–**6** (0.25 mM) in acetonitrile.
[c] Negative values are ligand reduction potential.
[d] Redox potentials correspond to Ru^{II}/Ru^{III} couple.
[e] Differential pulse voltammetry, scan rate, 5 mV s^{-1}; pulse height, 50 mV.

Table 3
Luminescence properties of the ruthenium complexes in the absence and presence of CT DNA (R = [DNA]/[Ru]).

Complexes	[a]λ_{excit} (nm)	[b]$\lambda_{emis\ (nm)}$ R = 0	R = 40	I/I_0	K_b (M)	n
$[Ru\ (5,6\text{-dmp})_2(dpq)]^{2+}$ **1**	448	594	600	4.6	$1.6\pm0.1\times10^6$	6.8
$[Ru\ (5,6\text{-dmp})_2(dppz)]^{2+}$ **2**	445	590	610	6.2	$1.8\pm0.1\times10^7$	2.0
$[Ru\ (5,6\text{-dmp})_2(dmdppz)]^{2+}$ **3**	453	590	592	1.8	$3.3\pm0.3\times10^5$	6.9
$[Ru\ (3,4,7,8\text{-tmp})_2(dpq)]^{2+}$ **4**	421	614	618	10.1	$3.0\pm0.2\times10^5$	7.9
$[Ru\ (3,4,7,8\text{-tmp})_2(dppz)]^{2+}$ **5**	424	586	616	2.2	$1.0\pm0.09\times10^6$	6.0
$[Ru\ (3,4,7,8\text{-tmp})_2(dmdppz)]^{2+}$ **6**	420	610	620	6.3	$6.0\pm0.3\times10^6$	7.9
$[Ru\ (bpy)_2(dpq)]^{2+}$	450	598	602	3.3	$1.2\pm0.09\times10^6$	8.9
$[Ru\ (phen)_2(dpq)]^{2+}$	447	592	598	3.1	$1.0\pm0.05\times10^6$	6.7

[a] Excitation wavelength maximum of the complexes.
[b] Emission wavelength maximum of the complexes in the presence and absence of CT DNA.

varies as **4**<**5**<**6**. On replacing the 5,6-dmp ligands in **2** by tmp as in **5**, a decrease in K_b value is observed as the bulky tmp co-ligands prevent the partial intercalation of dppz ligand. A similar decrease in DNA binding affinity is observed on going from **1** to **4**, supporting the importance of steric clash of tmp co-ligands with DNA. However, on going from **3** to **6** the K_b value increases because the latter with methyl groups on both the primary and co-ligands is involved in strong DNA groove binding (cf. above). This DNA binding mode also explains the inaccessibility of the MLCT excited state of **6** by water molecules,

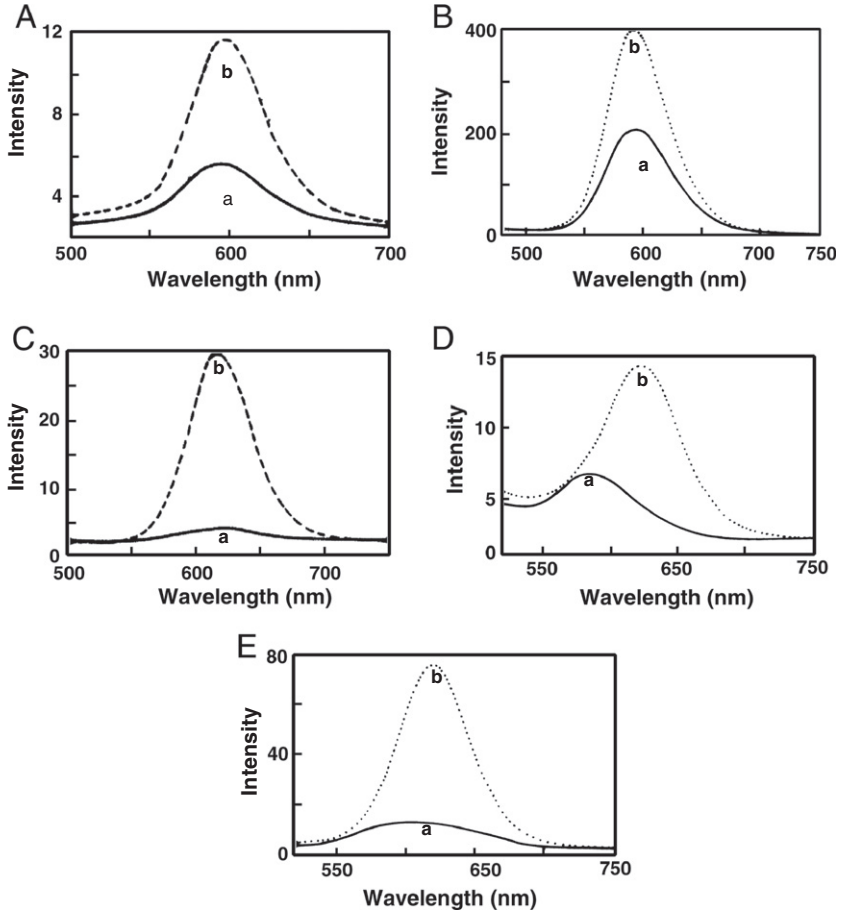

Fig. 2. (A) Emission spectra of the $[Ru(5,6\text{-dmp})_2(dpq)]^{2+}$(a) in the absence and presence (b) of CT DNA. (B) Emission spectra of the $[Ru(5,6\text{-dmp})_2(dmdppz)]^{2+}$(a) in the absence and presence (b) of CT DNA. (C) Emission spectra of the $[Ru(3,4,7,8\text{-tmp})_2(dpq)]^{2+}$(a) in the absence and presence (b) of CT DNA. (D) Emission spectra of the $[Ru(3,4,7,8\text{-tmp})_2(dppz)]^{2+}$ (a) in the absence and presence (b) of CT DNA. Emission spectra of the $[Ru(3,4,7,8\text{-tmp})_2(dmdppz)]^{2+}$ (a) in the absence and presence (b) of CT DNA at R value of 40.

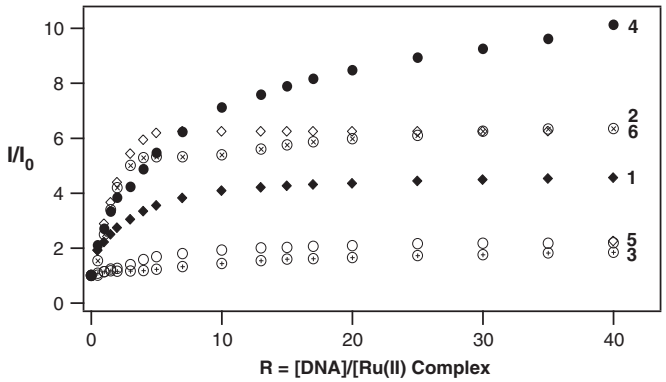

Fig. 3. Effect of addition of DNA on the emission intensity of the complexes **1**, 600; **2**, 590; **3**, 592; **4**, 618; **5**, 616; **6**, 620 nm in a 5% DMF/5 mM Tris–HCl/50 mM NaCl buffer at pH 7.1 and 25 °C, [Ru(II) complex] = 1×10^{-5} M.

leading to enhancement in emission for **6** higher than for **3** (cf. above). Thus the DNA binding affinity of the mixed ligand 5,6-dmp and tmp complexes varies depending upon the extent of hydrophobic interaction of the diimine ligands, as determined by the number of methyl substituents, and the number of aromatic rings in the other ligand.

2.4. Protein binding studies

2.4.1. Steady state emission

All the present Ru(II) complexes luminesce in aqueous solution (5% DMF/NaH_2PO_4:$NaHPO_4$ buffer at pH 7.1) upon irradiation in the MLCT band. Interestingly, on addition of BSA (5 μM), the emission intensity of the band (617–597 nm) observed for **2**, **4** and **5** increases 1.4–2.1 folds (Fig. 6, Table 4). This enhancement in emission intensity is attributed to the strong binding of the complexes in the

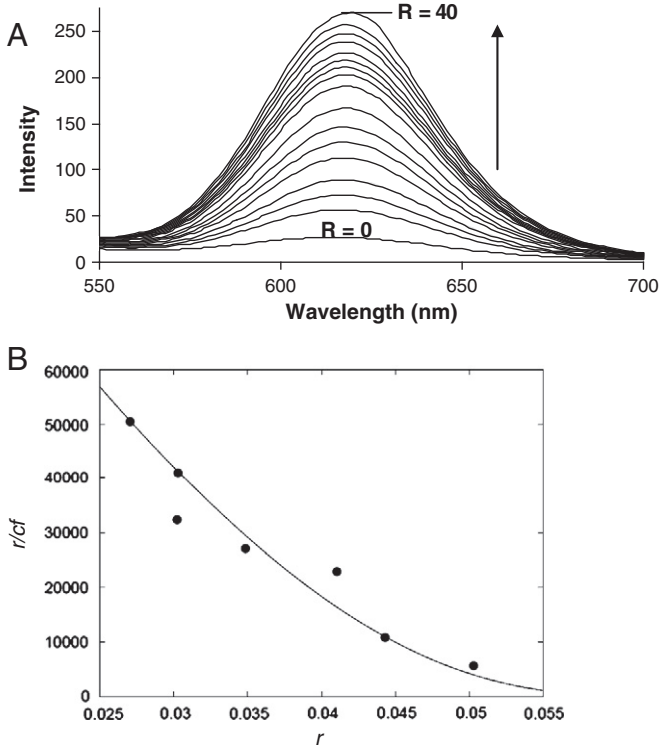

Fig. 4. (A) Emission spectra of [Ru(3,4,7,8-tmp)$_2$(dpq)]$^{2+}$ (1×10^{-5} M) in 5% DMF/5 mM Tris–HCl/50 mM NaCl buffer at pH 7.1 (R = [DNA]/[complex] = 0) and presence ($R = 1-40$) of increasing amounts of DNA. (B) Plot of r/c_f vs r for [Ru(3,4,7,8-tmp)$_2$(dpq)]$^{2+}$. The best fit line, superimposed on the data, according to McGhee and von Hippel Eqs. (2a), (2b) yields $K_b = 0.3\pm0.02\times10^6$ M^{-1} and $n = 7.9$.

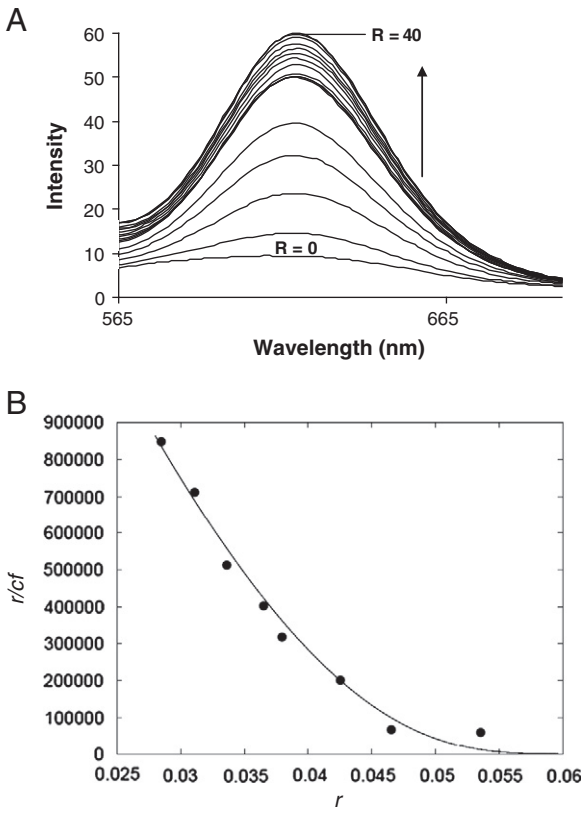

Fig. 5. (A) Emission spectra of [Ru (3,4,7,8-tmp)$_2$(dmdppz)]$^{2+}$ (1×10^{-5} M) in 5% DMF/5 mM Tris–HCl/50 mM NaCl buffer at pH 7.1 (R = [DNA]/[complex] = 0) and Presence ($R = 1-40$) of increasing amounts of DNA. (B) Plot of r/c_f vs r for [Ru (3,4,7,8-tmp)$_2$(dpq)]$^{2+}$. The best fit line, superimposed on the data, according to McGhee and von Hippel Eqs. (2a), (2b) yields $K_b = 6.0\pm0.3\times10^6$ M^{-1} and $n = 7.9$.

hydrophobic pocket of serum albumin [32]. Interestingly, the increase in emission intensity observed for the well-known DNA molecular light-switch complex [Ru(phen)$_2$(dppz)]$^{2+}$ under identical conditions is only 1.2. This reveals that methyl substitution on the phen ligand as in **2**, **4** and **5** increases the hydrophobicity and hence the protein binding efficiency of the complexes. Among the present methyl substituted complexes, [Ru(tmp)$_2$(dpq)]$^{2+}$ **4** exhibits a higher protein binding efficiency as the dpq ligand is involved in hydrophobic interaction. As **3** and **6** are precipitated upon adding BSA even at lower concentrations of the complexes, their protein binding affinity has not been determined.

2.5. Circular dichroic spectral measurements

Circular dichroic spectra provide information about the chirality of spectroscopically active species in solution. They are particularly sensitive to the degenerate/non-degenerate exciton coupling expected to arise when the same or two different chromophores are closely located in space to interact strongly. Thus *rac*–metal complexes give a zero CD and show induced circular dichroism (ICD) signals due to enantiopreferential binding, if any, providing further and definitive confirmation for their DNA binding [40]. Also, as CD signals are quite sensitive to the mode of DNA interactions of small molecules, the CD spectral technique is useful in diagnosing changes in DNA morphology during drug–DNA interaction [41,42]. Further, it is used to study the enantiopreferential DNA binding of metal complexes [17,40,43].

A solution of calf thymus DNA (2×10^{-5} M) exhibits a positive band (275 nm) due to base stacking and a negative band (248 nm) due to right-handed helicity of DNA. When the present *rac*-complexes are incubated with CT DNA at 1/R (=[Ru complex]/[DNA]) value of

unity, the CD spectrum of DNA undergoes changes in both the positive and negative bands (Table 5). Upon addition of *rac* complexes **1–6** (Figs. 7 and 8) to DNA both these bands disappear and an inverted CD signal is observed with intensity much higher than that for free DNA. This is typical of exciton coupled ICD arising due to ligand-ligand interactions among DNA bound/unbound complexes [26,27]. The complexes **1**, **2** [26] and **3** – **6** exhibit ICD upon interaction with different polynucleotides and the binding efficiency of DNA varies as CT DNA > poly(AT)$_{12}$ ≅ d(CGCGATCGCG)$_2$ > poly(GC)$_{12}$ (Figs. 7 and 8). All these observations reveal the preferential binding of all the complexes to AT and mixed rather than GC sequences.

2.6. Cytotoxicity of Ruthenium(II) complexes

The cytotoxicity of **1–6** against non-small lung carcinoma cell line (NCI-H460) has been investigated in comparison with the widely used drug cisplatin under identical conditions by using MTT assay. As revealed by the IC_{50} values (Table 6), interestingly, the cytotoxicity of 5,6-dmp complexes varies as **1**<**2**>**3** while that of tmp complexes varies as **4**<**5**<**6**, which is almost in line with the DNA binding affinities of the complexes (cf. above). Thus the complex [Ru(5,6-dmp)$_2$(dppz)]$^{2+}$ **2**, which exhibits the highest DNA binding affinity, displays potency higher than the other complexes for 24, 48 and 76 h incubation. Similarly, the complex [Ru(tmp)$_2$(dmdppz)]$^{2+}$ **6** exhibits cytotoxicity higher than all other complexes. Also, the complexes with hydrophobic ligands have the potential to bind with proteins strongly

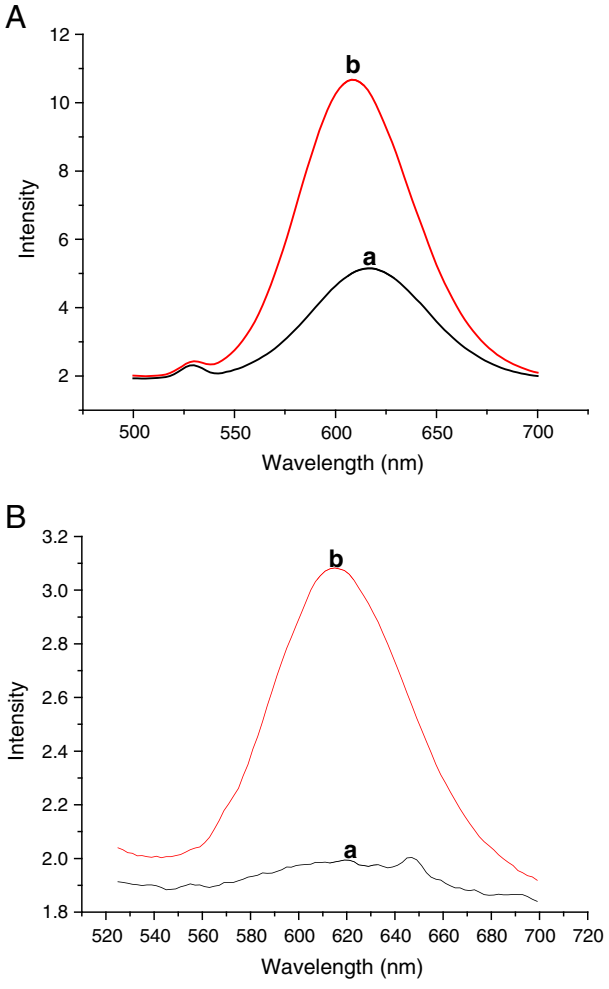

Fig. 6. (A) Emission spectra of the [Ru (3,4,7,8-tmp)$_2$(dpq)]$^{2+}$ (1×10^{-5} M) (a) in the absence and presence (b) of BSA. (B) Emission spectra of the [Ru (3,4,7,8-tmp)$_2$(dppz)]$^{2+}$ (1×10^{-5} M) (a) in the absence and presence (b) of BSA at R value of 1.5.

Table 4
Luminescence properties of the ruthenium complexes in the absence and presence of BSA protein (R = [BSA]/[complex]).

Complexes	[a]λ_{excit} (nm)	[b]λ_{emis} (nm)		I/I_0
		R = 0	R = 1.5	
[Ru (5,6-dmp)$_2$(dpq)]$^{2+}$ **1**	448	595	594	1.0
[Ru (5,6-dmp)$_2$(dppz)]$^{2+}$ **2**	445	590	592	1.4
[Ru (5,6-dmp)$_2$(dmdppz)]$^{2+}$ **3**	453	[c]–	–	–
[Ru (3,4,7,8-tmp)$_2$(dpq)]$^{2+}$ **4**	421	616	608	2.1
[Ru (3,4,7,8-tmp)$_2$(dppz)]$^{2+}$ **5**	424	617	615	1.6
[Ru (3,4,7,8-tmp)$_2$(dmdppz)]$^{2+}$ **6**	420	[c]–	–	–
[Ru (bpy)$_2$(dpq)]$^{2+}$	450	595	594	1.0
[Ru (phen)$_2$(dpq)]$^{2+}$	447	593	592	1.0

[a] Excitation wavelength maximum of the complexes.
[b] Emission wavelength maximum of the complexes in the presence and absence of BSA.
[c] The complex was precipitated during the addition of BSA.

[44] and cause severe inhibition of fundamental enzyme function in cancer surveillance. Further, the cytotoxicity of the present complexes is time dependent and varies with the mode and extent of their interaction with DNA, and is lower than that of cisplatin, which is known to bind to DNA covalently, unlike the present complexes.

2.7. Qualitative analysis of fluorescence of Ru(II) complexes in live and fixed cells

The luminescence enhancement observed upon binding of the present low cytotoxic Ru(II) complexes to DNA has been studied further to explore their use as fluorescent probes for DNA. The efficiency of the complexes as fluorescent probes for the detection of nuclear morphology has been analyzed by using fluorescent microscopy.

2.7.1. Cell morphology assessment

Organic fluorescent dyes such as acridine orange (AO), Hoechst 33258 (HO) and propidium iodide (PI) are among the most widely used fluorescent dyes to analyze cell viability. All these dyes are principally applied to enumerate the proportion of live and dead cells in a given population. Fluorescence-based cell viability stains are generally less hazardous and less expensive than radioisotopic techniques, and are also more sensitive than brightfield microscopy. These assays are reliable and easy to perform. Many popular fluorescence-based cell viability stains are classified into two major categories: (i) dye exclusion stains, which do not enter eukaryotic cells due to impermeablitiy of the cell membrane unless the plasma membrane is damaged and (ii) dye uptake by viable cells in which the cell membrane allows the dye to permeate into cytoplasm.

Despite the fact that fluorescence is observed for all the six complexes, the complex **4** alone is a better reagent as it has less background emission. All the other complexes produce stronger emission making the morphology cloaked for visualization. Also, **4** possess low cytotoxicity supporting its use as stains in cell-labeling techniques without harming

Table 5
CD parameters for the interaction of calf thymus DNA with complexes **1–6**.

Sample	[a]CD spectral band wavelength (nm)	
5 μM CT DNA	245	276
DNA + 5 μM [Ru(5,6-dmp)$_2$(dpq)]$^{2+}$ **1**	242, 282	260
DNA + 5 μM [Ru(5,6-dmp)$_2$(dppz)]$^{2+}$ **2**	242, 282	262
DNA + 5 μM [Ru(5,6-dmp)$_2$(dmdppz)]$^{2+}$ **3**	245, 285	267
DNA + 5 μM [Ru(3,4,7,8-tmp)$_2$(dpq)]$^{2+}$ **4**	245, 295	262
DNA + 5 μM [Ru(3,4,7,8-tmp)$_2$(dppz)]$^{2+}$ **5**	245, 280	265
DNA + 5 μM [Ru(3,4,7,8-tmp)$_2$(dmdppz)]$^{2+}$ **6**	249, 276	265

[a] Measurement made at 1/R value of 1 for complexes **1–6**. Where 1/R = [Ru]/[NP]; concentration of DNA solutions = 5×10^{-5} M. Cell path length = 1 cm.

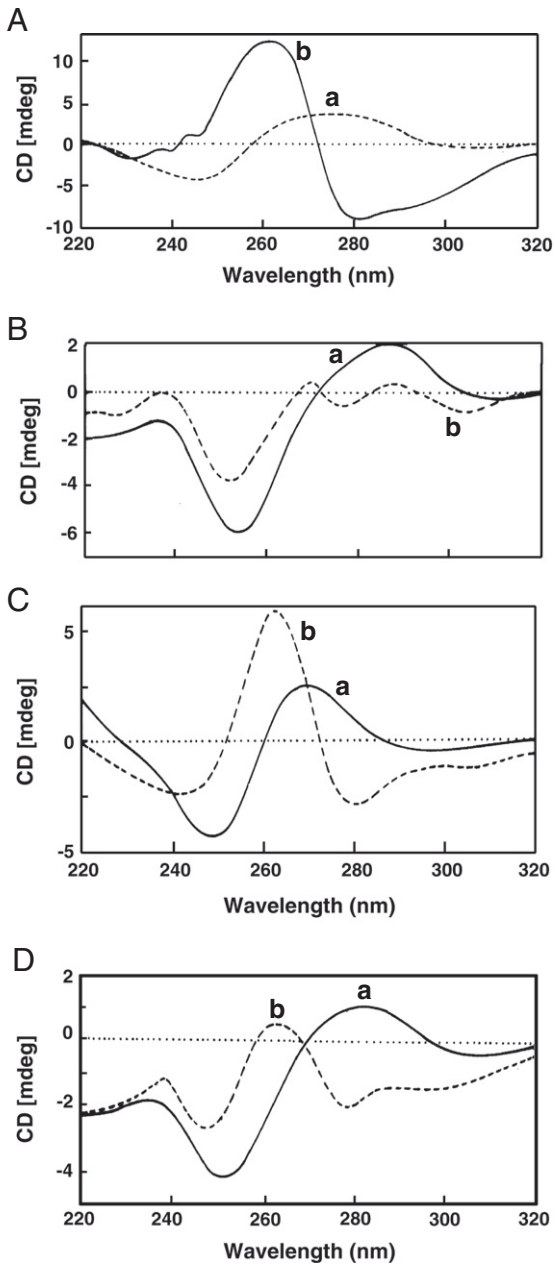

Fig. 7. (A) Circular dichroism spectra of CT DNA in the absence (a) and presence of $[Ru(5,6\text{-dmp})_2(dpq)]^{2+}$ at 1/R = 1; [DNA] = 2×10^{-5} M. (B) $poly(GC)_{12}$, (C) $poly(AT)_{12}$ and (D) $d(GTCGAC)_2$ in the absence (a) and presence of $[Ru(5,6\text{-dmp})_2(dpq)]^{2+}$ (b) at 1/R = 4; $poly(GC)_{12}$, $poly(AT)_{12}$ and $d(GTCGAC)_2 = 1\times10^{-5}$ M.

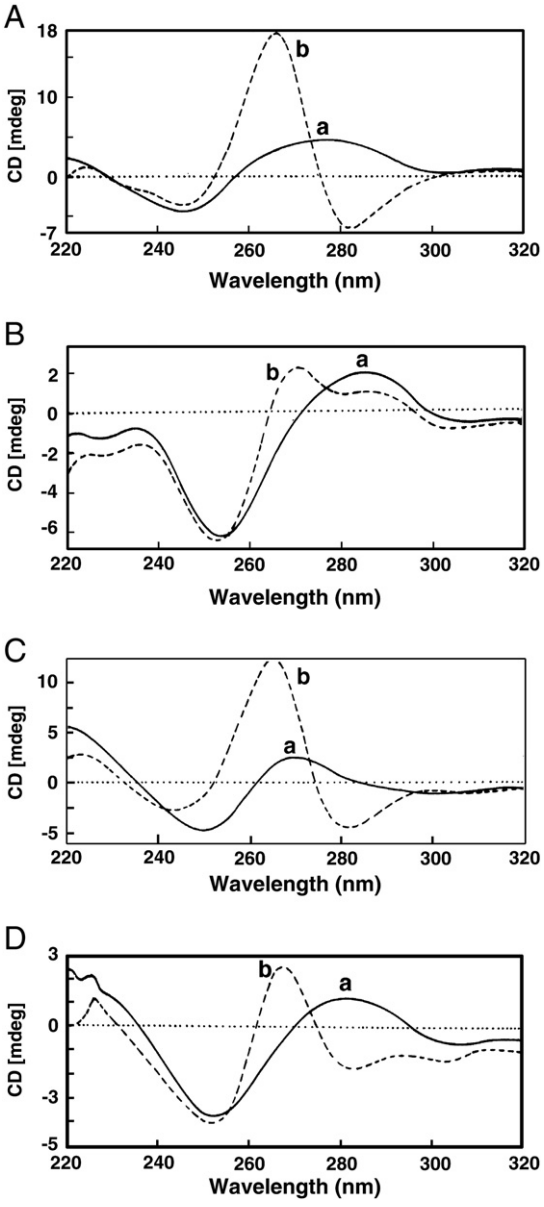

Fig. 8. (A) Circular dichroism spectra of CT DNA in the absence (a) and presence of $[Ru(3,4,7,8\text{-tmp})_2(dppz)]^{2+}$ at 1/R = 1; [DNA] = 2×10^{-5} M. (B) $poly(GC)_{12}$, (C) $poly(AT)_{12}$ and (D) $d(GTCGAC)_2$ in the absence (a) and presence of $[Ru(3,4,7,8\text{-dmp})_2(dppz)]^{2+}$ (b) at 1/R = 4; $poly(GC)_{12}$, $poly(AT)_{12}$ and $d(GTCGAC)_2 = 1\times10^{-5}$ M.

the cell. When it is exposed to fresh cell suspension, it does not enter the cytoplasm because of dye exclusion phenomenon and only a few cells emit red color fluorescence in fresh cell suspension (Figs. 9 (b), (c) Table 7). Therefore it is inferred that **4** can be used for cell viability assays. Comparative observation with phase contrast microscopy and AO/EB staining reveal the presence of monochromatic red fluorescence only in dead cells (Figs. 9 (a)–(c) Table 7). Interestingly, these stains have slow permeability through live cell membrane and have a fast affinity for dead cells and stain cytoplasm and nucleus, which help to visualize cell morphology of dead cells by fluorescence microscopy with standard filters. This finding also might be used to distinguish live from dead cells in a population. However, it is to be noted that the staining efficiency [45] of $[Ru(phen)_2(dppz)]^{2+}$ is lower than those of the known dyes AO/EB and Hoechst 33258.

2.7.2. Detection of fixed tissue sections

A variety of nuclear binding DNA dyes have been evaluated for detecting cell and nuclear structure abnormalities in tissue sections [46]. In this study, the complex **4** has been employed for their fluorescence specificity and sensitivity with cellular nucleus in paraffin-embedded tissue sections. Also, rat testis has been chosen as the tissue model as it has three different forms of nuclei such as germ cells (possessing tetraploid chromatin content, that is, after replication of DNA during M1 prophase), Leydig cells and Sertoli cells containing diploid nucleus, and sperm containing haploid nucleus, which helps us to interpret the specificities easily. Rehydrated paraffin sections were stained with **4**, and the nuclear structures were then classified (Figs. 9 (k), (l), Table 7). The cell morphologies correlate with the appearance of tissue sections stained with AO/EB (Fig. 9 (o), Table 7). Since **4** stains the tissue sections neatly and the nuclear details are clearly distinguished more than AO/EB, they have the possibility of finding application as a counterstain for immunofluorescence microscopy, permitting the identification of various

Table 6
In vitro cytotoxicity assays for complexes **1–6**, cisplatin non-small lung carcinoma (NCI-H460) cell line (data are mean ± SD of four replicates each).

Complex	[a]IC_{50} values (μM)		
	24 h	48 h	76 h
$[Ru(5,6\text{-dmp})_2(dpq)]^{2+}$ **1**	30.0 ± 1.5	24.5 ± 1.2	10.0 ± 0.9
$[Ru(5,6\text{-dmp})_2(dppz)]^{2+}$ **2**	11.5 ± 1.0	6.5 ± 1.2	6.5 ± 1.2
$[Ru(5,6\text{-dmp})_2(dmdppz)]^{2+}$ **3**	13.0 ± 0.8	8.0 ± 0.7	8.0 ± 0.7
$[Ru(3,4,7,8\text{-tmp})_2(dpq)]^{2+}$ **4**	22.5 ± 2.0	10.0 ± 1.0	10 ± 1.0
$[Ru(3,4,7,8\text{-dmp})_2(dppz)]^{2+}$ **5**	12.5 ± 1.5	10.0 ± 0.9	7.5 ± 0.8
$[Ru(3,4,7,8\text{-dmp})_2(dmdppz)]^{2+}$ **6**	7.5 ± 0.5	7.0 ± 0.5	7.0 ± 0.5
$[Ru(bpy)_2(dppz)]^{2+}$	42.0 ± 2.5	37 ± 1.7	30 ± 1.5
$[Ru(phen)_2(dppz)]^{2+}$	30.0 ± 2.0	20 ± 1.0	18 ± 0.5
Cisplatin	5.0 ± 0.5	1.0 ± 0.1	1.0 ± 0.1

[a] IC_{50} = concentration of drug required to inhibit growth of 50% of the cancer cells (in μM).

marker substances in specific cellular populations and the quantification of particular cell types in tissue sections adopting fluorescence microscopy.

2.7.3. Detection of fixed cell suspension staining

Recently, a variety of nucleic acid binding dyes have been developed [46] for fixed cell staining methods. In this study the complex **4** was examined as a dye to determine whether it would be suitable for cellular pathology study by adopting fluorescence microscopy. Three different cellular models were chosen for this study, in vitro cancer cells, human blood cells, and in vivo semen samples. They were fixed in ethanol and smears were stained with **4** and the fixed cell morphology detected is illustrated in Fig. 9 (b)–(j), Table 7. Specific emission was found in Human WBC cell types (e.g., neutrophils, eosinophils, basophils, lymphocyte and monocytes), cancer cells and also sperm heads with tails (Figs. 9 (e)–(h), Table 7). The nuclear morphology (Figs. 9 (m), (n), Table 7) reveals appreciable fluorescence emission and good binding efficiency in the tail region in comparison with AO/EB and Hoechst when a standard filter (blue) is used. Therefore, the complex **4** stains adequately in tail region, thereby permitting rapid scanning of sperm abnormalities to find out normal and defective sperms. When the DNA molecular light-switch complex $[Ru(phen)_2(dppz)]^{2+}$ is used to stain sperm cells, it exhibits specific staining property, staining only the head region of the sperm. In contrast, the complex **4**, which binds to DNA and protein through hydrophobic interaction, stains both the head and tail regions of the sperm. As the sperm head contains only nucleic acids, and the tail region only proteins [47], it is evident that **4** has the affinity to bind to the protein in the tail region as well as DNA in the head region. Clapham and his co-workers have reported that if an agent blocks the CatSper protein,

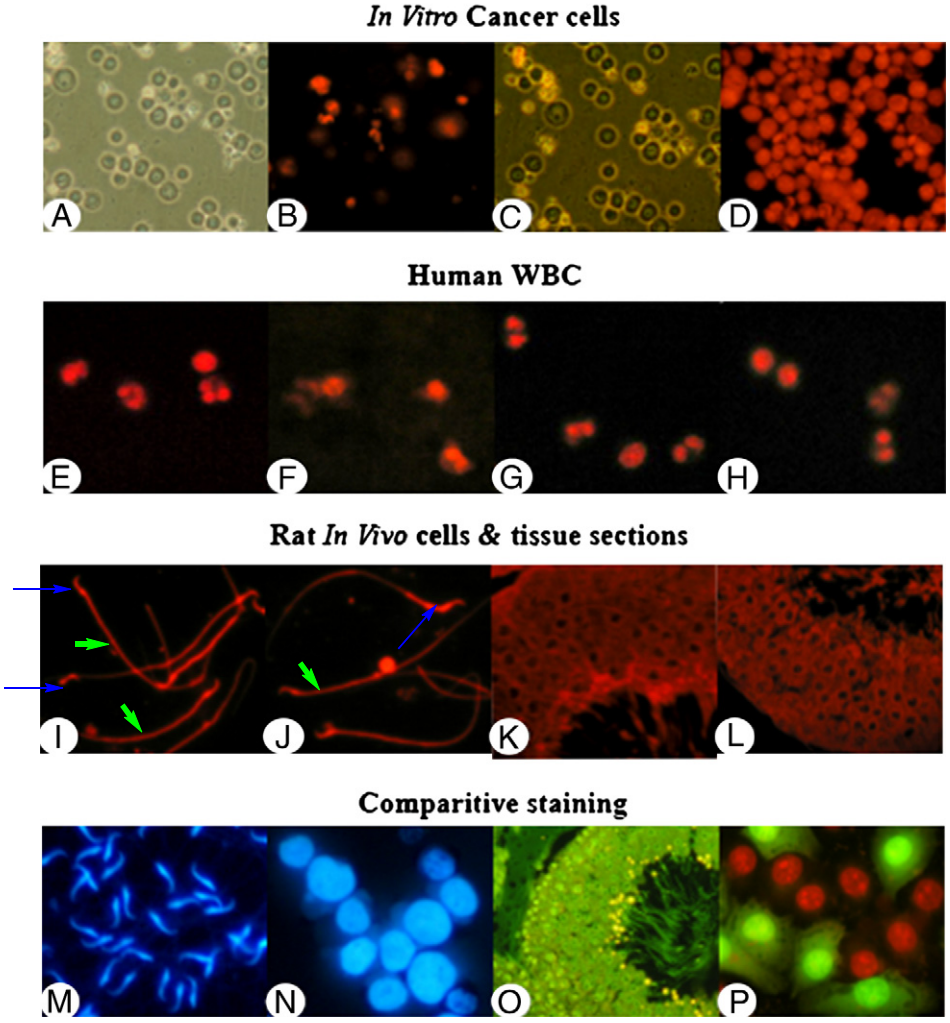

Fig. 9. Visualization of the morphology of *In vitro*, *in vivo* cells and tissues stained with $[Ru(3,4,7,8\text{-tmp})_2(dpq)]^{2+}$ **4** using fluorescent microscope (400× magnification). (a) *In vitro* cancer cells—phase contrast microscopy. (b) Unfixed fresh cells (dead cells stain red)—fluorescence microscopy. (c) Simultaneous visualization in phase contrast and fluorescence microscopy. (d) Ethanol fixed cells—fluorescent microscopy. (e–h) Human blood smear (nuclear lobules stain red). (i and j) Rat sperm (sperm heads (blue arrow) and tails (green arrow) stain red). (k and i) Rat testis tissue section. (m) Sperms stained by Hoechst. (n) *In vitro* cancer cells stained by Hoechst. (o) Testis section stained by acridine orange and ethidium bromide. (p) *In vitro* cancer cells stained by acridine orange and ethidium bromide.

Table 7
Optimum concentrations of ruthenium(II) complexes **1**–**6** used in various experiments in <1% EthOH/0.9% PBS Buffer (pH = 7.0).

Complex	Optimum concentrations	
	Morphology detection (μg/5 μl of cell suspension)	Comet assay (μg/comet gel)
$[Ru(5,6\text{-dmp})_2(dpq)]^{2+}$ **1**	0.49	1.46
$[Ru(5,6\text{-dmp})_2(dppz)]^{2+}$ **2**	0.41	1.22
$[Ru(5,6\text{-dmp})_2(dmdppz)]^{2+}$ **3**	0.42	1.26
$[Ru(3,4,7,8\text{-tmp})_2(dpq)]^{2+}$ **4**	0.35	0.70
$[Ru(5,6\text{-dmp})_2(dpppz)]^{2+}$ **5**	0.46	0.92
$[Ru(5,6\text{-dmp})_2(dmdppz)]^{2+}$ **6**	0.47	0.94

which is found exclusively in the tail of the sperm cell, then it would act as an effective non-hormonal contraceptive for both men and women [47]. So the complex **4** has the potential to act as a contraceptive under suitable conditions, and a deeper investigation on these protein binding complexes would pave the way for designing a promising non-hormonal metal-based contraceptive.

3. Conclusions

A series of mixed ligand ruthenium(II) complexes have been isolated by incorporating methyl substituents on the phen and dppz ligands in $[Ru(phen)_2(dpq)]^{2+}$ and $[Ru(phen)_2(dppz)]^{2+}$ complexes. All the complexes produce a detectable level of luminescence in aqueous solution in the absence of DNA and display substantial enhancement in luminescence on DNA binding. Among the dpq complexes the tmp complex exhibits a larger enhancement in luminescence upon binding to DNA and among the dppz and methyl-substituted dppz complexes the 5,6-dmp complex exhibits a higher DNA binding affinity suggesting the importance of ligand hydrophobic forces of interaction in DNA binding. All the complexes exhibit induced CD upon binding to CT DNA and a sequence specificity by binding to AT sequence more strongly than to GC sequence. It is noteworthy that upon increasing the number of methyl substituents on both the phen and dppz ligands the cytotoxicity of the complexes is increased. Interestingly, the $[Ru(tmp)_2(dpq)]^{2+}$ complex exhibits a higher enhancement in emission intensity when it binds with proteins and also stains proteins in the tail region of sperms. Our preliminary results reveal that the protein binding complex is expected to act as a contraceptive and this finding may pave the way for developing non-hormonal metal-based contraceptives. Thus the present study illustrates that increase in ligand hydrophobicity enhances on the DNA and protein binding abilities of Ru(II) complexes.

4. Experimental

4.1. Reagents and materials

$RuCl_3 3H_2O$ (Arora Matthey), 1,10-phenanthroline (Merck), 5,6-dimethyl-1,10-phenanthroline and 3,4,7,8-tetramethyl-1,10-phenanthroline (Aldrich), CT DNA (highly polymerized stored at 4 °C), Hoechst 33258 (Sigma) and cisplatin (Bristol-Myers Squibb Co., Princeton), the self-complementary oligonucleotides d(GCGCGCGCGCGC) referred as $d(GC)_{12}$, d(ATATATATATAT) referred as $d(AT)_{12}$, d(CGCGATCGCG) referred as $d(CGCGATCGCG)_2$ and protein BSA (bovine serum albumin, 66 kDa) were purchased from Sigma and stored at −20 °C. The lyophilized oligonucleotides were digested in Tris buffer and annealed using standard procedures to make the double-stranded oligonucleotides and stored at 4 °C. The concentrations of the oligonucleotide solutions were determined using the procedures provided by the supplier. Ultra-pure Milli-Q water (18.2 mX) was used in all experiments. Reagent grade solvents were dried and distilled by usual methods and the solvents were stored over molecular sieves (4 Å).

The cancer cell line NCI-H460 was obtained from National Centre for Cell Science (NCCS), Pune, India. The cells were cultured in RPMI 1640 medium (Sigma-Aldrich, St. Louis, MO, USA), as per the instruction by NCCS, supplemented with 10% fetal bovine serum (Sigma-Aldrich, St. Louis, MO, USA) and 100 U/mL penicillin and 100 μg/mL streptomycin as antibiotics (Himedia, Mumbai, India), in T25 cm^2, T75 cm^2, 6 well, 12 well, 24 well or 96 well culture plates (TPP, Switzerland), at 37 °C in a humidified atmosphere of 5% CO_2 in a CO_2 incubator (Heraeus, Hanau, Germany). All the experiments were performed by using cells from passage 15 or less.

Institutional Animal Ethics Committee (IAEC), established under the auspices of Committee for Purpose of Control and Supervision of Experiments on Animals (CPCSEA), Government of India, approved the experiment. Ninety-day-old Wistar strain male rats, raised from a stock obtained from the Indian Institute of Science, Bangalore, India, were used. Wistar rat was dissected under sodium pentobarbital anesthesia and the epididymis was removed. The cauda epididymal spermatozoa was taken and used for experimental purposes. Freshly prepared blood samples from healthy non-smoking donors at the University Biomedical center were used. The blood sampling has been approved by the Human Ethics Committee of the Bharathidasan University, India.

4.2. Methods and instrumentation

Microanalysis (C, H and N) were carried out with Vario EL elemental analyzer. An LCQ DECA XP electrospray mass spectrometer was employed for ESI-MS analysis. UV–Vis spectroscopy was recorded on a Varian Cary 300 Bio UV–Vis spectrophotometer using cuvettes of 1 cm path length. The ^1H NMR spectra were obtained at room temperature using a Bruker 400 MHz spectrometer. The chemical shift values in DMSO-d_6 are reported with respect to tetramethylsilane as the internal standard and the values are reported as: *d*-values (multiplicity, assignment).

Cyclic voltammetry and differential pulse voltammetry on a platinum sphere electrode were performed at 25.0 ± 0.2 °C. The temperature of the electrochemical cell was maintained by a cryocirculator (HAAKE D8-G). Voltammograms were generated with the use of an EG&G PAR Model 273 potentiostat. A Pentium IV computer along with EG&G M270 software was employed to control the experiments and acquire the data. A three-electrode system consisting of a platinum sphere (0.29 cm^2), a platinum auxiliary electrode and a reference electrode were used. The reference electrode for non-aqueous solution was $Ag(s)/Ag^+$, which consists of a Ag wire immersed in a solution of $AgNO_3$ (0.01 M) and tetra-*n*-butylammonium perchlorate (0.1 M) in acetonitrile placed in a tube fitted with a vycor plug using a sleeve [48]. The $E_{1/2}$ value observed under identical conditions for an Fc/Fc^+ couple in acetonitrile was 0.100 V with respect to the Ag/Ag^+ reference electrode. The cyclic voltammograms (CV) and differential pulse voltammograms (DPV) of **1**–**6** were obtained in MeCN solutions with 0.1 M $[(C_4H_9)_4N]ClO_4$ as the supporting electrolyte at ambient temperatures under N_2. Redox potentials were measured relative to a Ag/Ag^+ reference electrode. All the complexes are electroactive with respect to the metal as well as the ligand centers in the potential range of ±2.0 V. Emission intensity measurements were carried out using JASCO F 6500 spectrofluorometer. Circular dichroic spectra of DNA were obtained by using JASCO J-716 spectropolarimeter equipped with a peltier temperature control device. Visualization of the morphology of *in vitro*, *in vivo* cells and tissues stained by using fluorescent microscope 450–490 nm filter (Carl Zeiss, Jena, Germany).

Solutions of DNA in the buffer 50 mM NaCl/5 mM Tris HCl in water gave the ratio of UV absorbance at 260 nm and 280 nm, A_{260}/A_{280}, as 1.9 [49] indicating that the DNA was sufficiently free of protein. Concentrated stock solutions of DNA (13.5 mM) were prepared in buffer and sonicated for 25 cycles, where each cycle consisted of 30 s with 1 min intervals. The concentration of DNA in nucleotide phosphate (NP) was determined by UV absorbance at 260 nm after 1:100 dilutions.

The extinction coefficient, ε_{260}, was taken as 6600 M^{-1} cm^{-1}. Stock solutions were stored at 4 °C and used after more than 4 days or less. Concentrated stock solutions of metal complexes were prepared by dissolving calculated amounts of metal complexes in respective amount of solvent and diluted suitably with corresponding buffer to required concentrations for all the experiments.

4.3. Synthesis of ligands

The ligands dpq [50], dppz [51] and 11,12-dmdppz [51] were synthesized according to literature methods.

4.4. Synthesis of complexes

The complex $[Ru(5,6\text{-}dmp)_2(dppz)](PF_6)_2$ (**2**) was prepared as reported already [26].

The precursor complex *cis*-$[Ru(5,6\text{-}dmp)_2Cl_2]$ was synthesized according to literature methods [26] and *cis*-$[Ru(3,4,7,8\text{-}tmp)_2Cl_2]$ was synthesized using a procedure reported for the synthesis of $[Ru(bipy)_2Cl_2]$ [52].

4.4.1. Synthesis of $[Ru(5,6\text{-}dmp)_2(dpq)](PF_6)_2$ (1)

$[Ru(5,6\text{-}dmp)_2(dpq)](PF_6)_2$ was prepared by refluxing the precursor *cis*-$[Ru(5,6\text{-}dmp)_2Cl_2]$ (1 mmol) and dpq (1.1 mmol) in 50 mL of 75% ethanol for 8 h. The reaction volume was then reduced (20 mL), the solution was cooled, and excess KPF_6 was added to it. The resultant orange precipitate was filtered off and washed with water (100 mL) and then ether (50 mL). The solid was dissolved in acetonitrile (20 mL) and applied to the head of a column of activated aluminum oxide (neutral Brockmann 1). The orange band was eluted with acetonitrile. Yield, 0.31 g, 79%. Anal. Calc. for $C_{28}H_{20}N_6P_2F_{12}Ru$: C, 40.45, H, 2.42, N, 10.11. Found: C, 40.25, H, 2.32, N, 10.06. ESI-MS: $[Ru(5,6\text{-}dmp)_2(dpq)]^{2+}$ displays a peak at m/z = 375.40, calculated = 374.92. ^1H NMR (DMSO-d_6, 400 MHz): δ (multiplicity, integration, assignment, J/Hz, coordination-induced shifts: c.i.s., $\delta_{complex}-\delta_{ligand}$), ppm 5,6-dmp, 8.15 (d, 2 H, H_2, 5.1, −0.93), 7.77 (t, 2 H, H_3, 5.1, 0.21), 8.88 (d, 2 H, H_4, 7.5, 0.58), 8.84 (d, 2 H, H_7, 7.3, 0.53), 7.58 (t, 2 H, H_8, 4.9, 0.02), 8.10 (d, 2 H, H_9, 5.0, −0.98), 2.87 (s, 12 H, 5,6-CH_3, 0.30); dpq, 8.33 (d, 2 H, H_2, 7.5, −1.10), 7.921 (t, 2 H, H_3, 4.8, 0.002), 9.53 (d, 2 H, H_4, 7.5, 0.31), 9.39 (s, 2 H, H_6, 0.25). The chloride salt was prepared from their PF_6 salt by precipitating it from an acetone solution of the PF_6 salt with tetra-*n*-butylammonium chloride.

4.4.2. Synthesis of $[Ru(5,6\text{-}dmp)_2(11,12\text{-}dmdppz)](PF_6)_2$ (3)

The complex $[Ru(5,6\text{-}dmp)_2(11,12\text{-}dmdppz)](PF_6)_2$ was prepared by refluxing the precursor *cis*-$[Ru(5,6\text{-}dmp)_2Cl_2]$ (1 mmol) and dmdppz (1.1 mmol) in 75% ethanol (50 mL) for 8 h. The volume was then reduced to 20 mL, the solution was cooled, and excess KPF_6 was added. The resultant orange precipitate was filtered off, washed with water (100 mL) and then ether (50 mL). The product was dissolved in acetonitrile (20 mL) and applied to the head of a column of activated aluminum oxide (neutral Brockmann 1). The orange band was eluted with acetonitrile. Yield, 0.31 g, 79%. Anal. Calc. for $C_{34}H_{26}N_6P_2F_{12}Ru$: C, 44.89, H, 2.88, N, 9.24. Found: C, 44.55, H, 2.82, N, 9.16. ESI-MS: $[Ru(5,6\text{-}dmp)_2(dmdppz)]^{2+}$ displays a peak at m/z = 413.50, calculated = 413.90. ^1H NMR (DMSO-d_6, 400 MHz): δ (multiplicity, integration, assignment, J/Hz, coordination-induced shifts: c.i.s., $\delta_{complex}-\delta_{ligand}$), ppm: 5,6-dmp, 8.200 (d, 2H, H_2, 5.6, −0.891), 7.87 (t, 4H, H_3 and H_8, 4.1, 0.315), 8.53 (d, 2H, H_4, 6.8, 0.220), 8.50 (d, 2H, H_7, 6.4, 0.198), 8.18 (d, 2H, H_9, 5.6, −0.913), 2.49 (s, 6H, 5-CH_3, −0.084), 2.22 (s, 6H, 6-CH_3, −0.351); 11,12-dmdppz, 8.09 (d, 2H, H_2 and H_2', 5.4, −1.114), 7.72 (t, 2H, H_3 and H_3', 4.0, −0.230), 9.56 (d, 2H, H_4 and H_4', 7.2, 0.033), 8.48 (s, 2H, H_7 and H_7', 0.309), 2.77 (s, 6H, 8,8′-CH_3, 0.179). The chloride salt was prepared from their PF_6 salt by precipitating it from an acetone solution of the PF_6 salt with tetra-*n*-butylammonium chloride.

4.4.3. Synthesis of $[Ru(3,4,7,8\text{-}tmp)_2(dpq)](PF_6)_2$ (4)

$[Ru(3,4,7,8\text{-}tmp)_2(dpq)](PF_6)_2$ was prepared by refluxing the precursor *cis*-$[Ru(3,4,7,8\text{-}tmp)_2Cl_2]$ (1 mmol) and dpq (1.1 mmol) in 50 mL of 75% ethanol for 8 h. The volume was then reduced (20 mL), the solution was cooled, and excess KPF_6 was added. The resultant orange precipitate was filtered off washed with water (100 mL) and then ether (50 mL). The solid was dissolved in acetonitrile (20 mL) and applied to the head of a column of activated aluminum oxide (neutral Brockmann 1). The orange band was eluted with acetonitrile. Yield, 0.31 g, 79%. Anal. Calc. for $C_{30}H_{24}N_6P_2F_{12}Ru$: C, 41.92, H, 2.81, N, 9.78. Found: C, 41.55, H, 2.72, N, 9.56. ESI-MS: $[Ru(3,4,7,8\text{-}tmp)_2(dpq)]^{2+}$ displays a peak at m/z = 409.50, calculated = 409.90. ^1H NMR (DMSO-d_6, 400 MHz): δ (multiplicity, integration, assignment, J/Hz, coordination-induced shifts: c.i.s., $\delta_{complex}-\delta_{ligand}$), ppm 3,4,7,8-tmp, 8.475 (s, 4H, H_2 and H_9, −0.404), 7.80 (d, 2H, H_5, 5.1, −0.057), 7.71 (d, 2H, H_6, 4.8, −0.152), 2.22 (s, 6H, 3-CH_3, −0.223), 2.20 (s, 6H, 8-CH_3, −0.244), 2.77 (s, 12H, 4,7-CH_3, 0.215); dpq, 8.10 (d, 2H, H_2, 5.1, −1.329), 7.86 (t, 2H, H_3, 4.2, −0.061), 9.47 (d, 2H, H_4, 7.5, 0.246), 9.36 (s, 2H, H_6, 0.229). The chloride salt was prepared from their PF_6 salt by precipitating it from an acetone solution of the PF_6 salt with tetra-*n*-butylammonium chloride.

4.4.4. Synthesis of $[Ru(3,4,7,8\text{-}tmp)_2(dppz)](PF_6)_2$ (5)

$[Ru(3,4,7,8\text{-}tmp)_2(dpq)](PF_6)_2$ was prepared by refluxing the precursor *cis*-$[Ru(3,4,7,8\text{-}tmp)_2Cl_2]$ (1 mmol) and dpq (1.1 mmol) in 50 mL of 75% ethanol for 8 h. The volume was then reduced (20 mL), the solution was cooled, and excess KPF_6 was added. The resultant orange precipitate was filtered off and washed with water (100 mL) and then ether (50 mL). The solid was dissolved in acetonitrile (20 mL) and applied to the head of a column of activated aluminum oxide (neutral Brockmann 1). The orange band was eluted with acetonitrile. Yield, 0.31 g, 79%. Anal. Calc. for $C_{34}H_{26}N_6P_2F_{12}Ru$: C, 44.89, H, 2.88, N, 9.24. Found: C, 44.55, H, 2.70, N, 9.16. ESI-MS: $[Ru(3,4,7,8\text{-}tmp)_2(dppz)]^{2+}$ displays a peak at m/z = 428.47, calculated = 428.01. ^1H NMR (DMSO-d_6, 400 MHz): δ (multiplicity, integration, assignment, J/Hz, coordination-induced shifts: c.i.s., $\delta_{complex}-\delta_{ligand}$), ppm 3,4,7,8-tmp, 8.48 (s, 4H, H_2 and H_9, −0.398), 7.72 (s, 4H, H_5 and H_6, −0.143), 2.23 (s, 12H, 3,8-CH_3, −0.222), 2.77 (s, 12H, 4,7-CH_3, 0.218); dppz, 8.06 (d, 2H, H_2, 5.1, −1.397), 7.84 (t, 2H, H_3, 4.6, −0.067), 9.47 (d, 2H, H_4, 8.1, 0.286), 8.21 (s, 2H, H_7, −0.119), 7.87 (s, 2H, H_8, −0.144). The chloride salt was prepared from their PF_6 salt by precipitating it from an acetone solution of the PF_6 salt with tetra-*n*-butylammonium chloride.

4.4.5. Synthesis of $[Ru(3,4,7,8\text{-}tmp)_2(11,12\text{-}dmdppz)](PF_6)_2$ (6)

$[Ru(3,4,7,8\text{-}tmp)_2(11,12\text{-}dmdppz)](PF_6)_2$ was prepared by refluxing the precursor *cis*-$[Ru(3,4,7,8\text{-}tmp)_2Cl_2]$ (1 mmol) and dmdppz (1.1 mmol) in 50 mL of 75% ethanol for 8 h. The volume was then reduced (20 mL), the solution was cooled, and excess KPF_6 was added. The resultant orange precipitate was filtered off and washed with water (100 mL) and then ether (50 mL). The solid was dissolved in acetonitrile (20 mL) and applied to the head of a column of activated aluminum oxide (neutral Brockmann 1). The orange band was eluted with acetonitrile. Yield, 0.31 g, 79%. Anal. Calc. for $C_{36}H_{30}N_6P_2F_{12}Ru$: C, 46.11, H, 3.22, N, 8.96. Found: C, 46.00, H, 3.10, N, 8.66. ESI-MS: $[Ru(3,4,7,8\text{-}tmp)_2(dmdppz)]^{2+}$ displays a peak at m/z = 442.47, calculated = 442.03. ^1H NMR (DMSO-d_6, 400 MHz): δ (multiplicity, integration, assignment, J/Hz, coordination-induced shifts: c.i.s., $\delta_{complex}-\delta_{ligand}$), ppm 3,4,7,8-tmp, 8.905 (s, 1H, H_2, 0.026), 8.88 (s, 1H, H_2', 0.002), 8.09 (d, 2H, H_5, 5.1, 0.232), 7.96 (d, 2H, H_6, 4.8, 0.094), 8.86 (s, 1H, H_9, −0.019), 8.83 (s, 1H, H_9', −0.047), 2.82 (s, 12H, 3,8-CH_3, 0.369), 2.84 (s, 12H, 4,7-CH_3, 0.289); 11,12-dmdppz, 8.34 (d, 1H, H_2, 5.4, −0.865), 8.21 (d, 1H, H_2', 5.1, −0.998), 7.90 (t, 1H, H_3, 5.0, −0.050), 7.75 (t, 1H, H_3', 4.6, −0.198), 9.57 (d, 1H, H_4, 5.4, 0.040), 9.55 (d, 1H, H_4', 5.4, 0.016), 8.27 (s, 2H, H_7 and H_7', 0.101), 2.64 (s, 6H, 8,8′-CH_3, 0.041). The chloride salt was prepared from their PF_6 salt by precipitating it

from an acetone solution of the PF_6 salt with tetra-*n*-butylammonium chloride.

4.5. ^1H NMR spectra

To throw light on the nature of metal–ligand bonding and conformation of chelate rings of mononuclear Ru(II) complexes in dimethyl sulfoxide solutions, the chemical shifts of the free and coordinated ligands are summarized in the experimental section, along with coordination-induced shifts (c.i.s. $= \delta_{complex} - \delta_{ligand}$) and coupling constants [53–55]. Spectral assignments [56–58] were made on the basis of COSY spectra of the complexes and the *J* values are consistent with the assignment.

The ^{1}H NMR spectra of mononuclear complexes show seven (**4**,**5**) or ten (**1**,**3**) or 14 (**6**) aromatic signals and one (**1**) or two (**5**) or three (**3**,**4**,**6**) aliphatic signals due to the substitution of methyl groups indicating the presence of C_2 symmetry in all the complexes. It is clear that the aromatic protons in the coordinated 5,6-dmp (**1**,**3**) and 3,4,7,8-tmp (**4**,**5**), dpq (**1**,**4**), 11,12-dmdppz (**3**) and dppz (**5**) are magnetically equivalent while 3,4,7,8-tmp (**6**) and 11,12-dmdppz (**6**) are magnetically non-equivalent due to the steric crowding imposed by both the ligands in the octahedral environment. When coordinated to Ru(II) the three five-membered chelate rings are expected to exist in envelope conformation. The aliphatic protons of methyl groups in the 5,6- (**3**) and 3,8- (**4**) positions are magnetically equivalent while 3,8- (**5**) position is magnetically non-equivalent show upfield shifts indicating the importance of π-back donation, which would increase the electron density at these positions. On the other hand, the methyl groups in the 5,6- (**1**), 3,8- (**6**), 4,7- (**4**,**5**) and 8,8′- (**3**, **6**) positions are magnetically equivalent and exhibit downfield shift due to metal-to-ligand σ-donation.

The aromatic H_2 and H_9 protons of 5,6-dmp (**1**,**3**) and 3,4,7,8-tmp (**4**,**5**), H_2 proton of dpq (**1**,**4**), dppz (**5**) and H_2 and H_2' proton of 11,12-dmdppz (**6**) exhibit negative c.i.s. values, which are adjacent to the coordinated nitrogen resulting from through-space ring-current anisotropy effects since on coordination these protons lie directly over the shielding plane of another aromatic py ring. The H_3 proton of 11,12-dmdppz (**3**,**6**), dpq (**4**) and dppz (**5**) also show negative c.i.s. value due to the magnetic anisotropy induced by proximate ring current; however the influence of the latter on H_4 proton of 11,12-dmdppz (**3**,**6**), dpq (**4**) and dppz (**5**) is affected less. The H_5 and H_6 protons of 3,4,7,8-tmp (**4**,**5**) shifted upfield due to Ru(II) to ligand π-back donation. The positive c.i.s. values observed for H_3, H_4, H_7 and H_8 protons of 5,6-dmp (**1**,**3**), H_5 and H_6 protons of 3,4,7,8-tmp (**6**), H_4 and H_6 protons of dpq (**1**,**4**), H_4 and H_7 protons of dppz (**5**) and 11,12-dmdppz (**3**,**6**) indicate the importance of σ-donation of electrons to Ru(II) *via* the nitrogen lone pairs. Further, the ^{1}H NMR spectra of **1** and **3**–**6** show only single resonances for all the aromatic protons, substantiating the possibility of the presence of Λ and Δ enantiomers in equal proportions and thus a racemic mixture of **1** and **3**–**6** is obtained.

4.6. DNA binding experiments

Concentrated stock solutions of metal complexes were prepared by dissolving them in 5% DMF/5 mM Tris–HCl/50 mM NaCl buffer at pH 7.1 of metal complexes and diluting suitably with corresponding buffer to required concentrations for all the experiments. For emission spectral experiments the DNA solutions were pretreated with the solutions of metal complexes to ensure no change in concentration of the metal complexes. Emission measurements were carried out by using a Hitachi F 4500 spectrofluorimeter. 5% DMF/5 mM Tris–HCl/50 mM NaCl buffer at pH 7.1 was used as a blank to make preliminary adjustments. The excitation wavelength was fixed and the emission range was adjusted before measurements. All measurements were made at 25 °C in a thermostated cuvette holder with 5 nm entrance slit and 5 nm exit slit. For emission spectral titrations 1.0×10^{-5} M concentration of ruthenium solutions were used and CT DNA was added in steps till R = 40. The emission enhancement factors were measured by comparing the intensities at the emission spectral maxima in the absence and presence of DNA, under similar conditions. The emission decay measurements of the DNA-bound complexes (R = 40) were carried out using the time correlated single photon counting technique (TCSPC) by exciting the sample at 445 nm (Model 5000U, LED, IBH, UK) with micro channel plate photomultiplier tube (MCP-PMT) as detector. Emission titration data were analyzed using McGhee von Hippel equation using non-co-operative binding model and non-linear least square analysis.

Circular dichroic spectra of DNA were obtained by using JASCO J-716 spectropolarimeter equipped with a peltier temperature control device. All experiments were done using a quartz cell of 1 or 0.2 cm path length. Each CD spectrum was collected after averaging over at least 4 accumulations using a scan speed of 100 nm min^{-1} and a 1 s response time. Machine plus cuvette baselines were subtracted and the resultant spectrum zeroed 50 nm outside the absorption bands. Cyclic voltammetry (CV) and differential pulse voltammetry (DPV) were performed in a single compartment cell with a three electrode configuration on a EG&G PAR 273 potentiostat–galvanostat equipped with an PIV computer. The working electrode was a glassy carbon disk (0.384 cm^2) and the reference electrode a saturated calomel electrode. A platinum plate was used as the counter electrode. The supporting electrolyte was 50 mM NaCl/5 mM Tris–HCl buffer at pH 7.1. Solutions were deoxygenated by purging with nitrogen gas for 15 min prior to measurements; during measurements a stream of N_2 gas was passes over the solution. All the experiments were carried out at 25.0 ± 0.2 °C maintained by a Haake D8-G circulating bath. The redox potential $E_{1/2}$ was calculated from the anodic (E_{pa}) and cathodic (E_{pc}) peak potentials of CV traces as $(E_{pa} + E_{pc})/2$ and also from the peak potential (E_{pa}) of DPV response as $E_p + \Delta E/2$ (ΔE is the pulse height).

4.7. Protein binding experiments

Steady-state emission studies of the ruthenium(II) complexes were carried out by addition of the concentration of BSA (1.5×10^{-5} M) while keeping the concentration of metal complex constant. Concentrated stock solutions of metal complexes were prepared by dissolving them in 5% DMF/NaH_2PO_4:$NaHPO_4$ buffer at pH 7.1 of metal complexes and diluting suitably with corresponding buffer to required concentrations for all the experiments. For emission spectral experiments the protein solutions were pretreated with the solutions of metal complexes to ensure no change in concentration of the metal complexes. Emission measurements were carried out by using a Hitachi F 4500 spectrofluorimeter. 5% DMF/NaH_2PO_4:$NaHPO_4$ buffer at pH 7.1 was used as a blank to make preliminary adjustments. The excitation wavelength was fixed and the emission range was adjusted before measurements. All measurements were made at 25 °C in a thermostated cuvette holder with 5 nm entrance slit and 5 nm exit slit.

4.8. Fixed cell staining

The monolayer culture of NCI-H460 cells were harvested at exponential phase, human blood was collected from the vein [59] and 90 days old Wistar rat was dissected under sodium pentobarbital anaesthesia and the epididymis were removed. The cauda epididymal spermatozoa was taken. The cells were fixed with 70% ethanol and cells washed with cold phosphate buffered saline, and incubated with Ru complex (Table 6) in buffer for 5–10 min at room temperature in the dark. Cells were then washed with buffer followed immediately by observation using a fluorescent microscope using 450–490 nm filter (Carl Zeiss, Jena, Germany).

4.9. Cell viability assay

MTT assay was carried out as described previously [60]. The complexes **1**–**5**, in the concentration 0.05–100 μM, dissolved in DMSO (Sigma-Aldrich, St. Louis, MO, USA), were added to the wells 24 h after

seeding of 5×10^3 cells per well in 200 μL of fresh culture medium. DMSO was used as the vehicle control. After 24 and 48 h, 20 μL of MTT solution [5 mg/mL in phosphate-buffered saline (PBS)] was added to each well and the plates were wrapped with aluminum foil and incubated for 4 h at 37 °C. The purple formazan product was dissolved by addition of 100 μL of 100% DMSO to each well. The absorbance was monitored at 570 nm (measurement) and 630 nm (reference) using a 96 well plate reader (Bio-Rad, Hercules, CA, USA). The stock solutions of the metal complexes were prepared in DMSO and in all the experiments the percentage of DMSO was maintained in the range of 0.1–1%. DMSO by itself was found to be non-toxic to the cells till 1% concentration. Data were collected for four replicates each and used to calculate the mean. The percentage inhibition was calculated, from this data, using the formula:

$$= \frac{\text{Mean OD of untreated cells (control)} - \text{Mean OD of treated cells}}{\text{Mean OD of untreated cells (control)}} \times 100$$

The IC_{50} values were calculated using Table Curve 2D version 5.01

Abbreviations

AO	acridine orange
BSA	bovine serum albumin
CT DNA	calf thymus
cpdppz	12-cyano-12,13-dihydro-11*H*-cyclopenta[b]dipyrido[3,2-*h*:2′ 3′-*j*]phenazine-12-carbonyl
CPCSEA	Committee for Purpose of Control and Supervision of Experiments on Animals
5,6-dmp	5,6-dimethyl-1,10-phenanthroline
11,12-dmdppz	11,12-dimethyl-dipyrido[3,2-*a*:2′,3′-*c*]phenazine
dip	4,7-diphenyl-1,10-phenanthroline
4,7-dmp	4,7-dimethyl-1,10-phenanthroline
2,9-dmp	2,9-dimethyl-1,10-phenanthroline
4,4′-dmb	4,4′-dimethyl-2,2′-bipyridine
dpq	dipyrido-[3,2-*d*:2′,3′-*f*]-quinoxaline
dppz	dipyrido[3,2-*a*:2′,3′-*c*]phenazine
flone	4,5-diazafluorene-9-one
DMF	dimethylformamide
MTT	(3-(4,5-Dimethylthiazol-2-yl)-2,5-diphenyltetrazolium bromide
EB	ethidium bromide
ESI-MS	electrospray ionization mass spectrometry \
HO	Hoechst 33258
H(tdp)	2-[(2-(2-hydroxyethylamino)ethylimino)methyl] phenol
ip	imidazo[4,5-*f*] [1,10] phenanthroline
IAEC	Institutional Animal Ethics Committee
ICD	induced circular dichroism
MCP-PMT	micro channel plate photomultiplier tube
MLCT	metal-to-ligand charge transfer transition
10-mdppz	11-methyldipyrido[3,2-a:2′,3′-c]phenazine
NCCS	National Centre for Cell Science
tmp	3,4,7,8-tetramethyl-1,10-phenanthroline
TCSPC	time correlated single photon counting technique
PBS	phosphate-buffered saline
PI	propidium iodide

Acknowledgments

Council of Scientific and Industrial Research, New Delhi, India (Grant No. 01(2101)/07/EMR-II) is gratefully acknowledged for financial support. Professor M. Palaniandavar is a recipient of Ramanna Fellowship, Department of Science and Technology, New Delhi, India.

References

[1] D.S. Sigman, Acc. Chem. Res. 19 (1986) 180–186.
[2] S.M. Hecht, Acc. Chem. Res. 19 (1986) 383–391.
[3] A.M. Pyle, E.C. Long, J.K. Barton, J. Am. Chem. Soc. 11 (1989) 4520–4522.
[4] A.M. Pyle, T. Morii, J.K. Barton, J. Am. Chem. Soc. 112 (1990) 9432–9434.
[5] H. Szmacinski, E. Terpetschnig, J.R. Lakowicz, Biophys. Chem. 62 (1996) 109–120.
[6] C.S. Chow, J.K. Barton, Methods Enzymol. 212 (1992) 219–242.
[7] B. Norden, P. Lincoln, B. Akerman, E. Tuite, Metals in Biological systems, vol.33, 1996 (Edited by Sigel, A and Sigel, H), pp.177-252. Marcel Dekker, New Yark.
[8] R.T. Belly, A. E. Friedman, (1994), RD Patent 357023.
[9] A.E. Friedman, J.C. Chambron, J.P. Sauvage, N.J. Turro, J.K. Barton, J. Am. Chem. Soc. 112 (1990) 4960–4962.
[10] Y. Jenkins, A.E. Friedman, N.J. Turro, J.K. Barton, Biochemistry 31 (1992) 10809–10816.
[11] R.M. Hartshorn, J.K. Barton, J. Am. Chem. Soc. 114 (1992) 5919–5925.
[12] C.A. Puckett, J.K. Barton, J. Am. Chem. Soc. 129 (2007) 46–47.
[13] B. Onfelt, P. Lincoln, B. Norden, J. Am. Chem. Soc. 123 (2001) 3630–3637.
[14] B. Onfelt, P. Lincoln, B. Norden, J. Am. Chem. Soc. 121 (1999) 10846–10847.
[15] C.J. Murphy, M.R. Arkin, Y. Jenkins, N.D. Gathlia, S.H. Bossmann, N.J. Turro, J.K. Barton, Science 262 (1993) 1025–1029.
[16] M.R. Arkin, E.D.A. Stemp, R.E. Holmlin, J.K. Barton, A. Hormann, E.J.C. Olson, P.F. Barbara, Science 273 (1996) 475–480.
[17] S. Delaney, M. Pascaly, P. Bhattarcharya, K. Han, J.K. Barton, Inorg. Chem. 41 (2002) 1966–1974.
[18] E. Ruba, J.R. Hart, J.K. Barton, Inorg. Chem. 43 (2004) 4570–4578.
[19] M.E. Jiménez-Hernández, G. Orellana, F. Montero, M.T. Portolés, Photochem. Photobiol. 72 (2000) 28–34.
[20] B. Onfelt, L. Gostring, P. Lincoln, P. Norden, A. Onfelt, Mutagen. 17 (2002) 317–320.
[21] E.D.A. Stemp, M.K. Arkin, J.K. Barton, J. Am. Chem. Soc. 117 (1995) 2375–2376.
[22] J.G. Liu, Q.L. Zhang, X.F. Shi, L.N. Ji, Inorg. Chem. 40 (2001) 5045–5050.
[23] R.B. Nair, E.S. Teng, S.L. Kirkland, C.J. Murphy, Inorg. Chem. 37 (1998) 139–141.
[24] J.G. Liu, B.H. Ye, H. Li, L.N. Ji, R.H. Li, J.Y. Zhou, J. Inorg. Biochem. 73 (1999) 117–122.
[25] L.N. Ji, X.H. Zon, J.G. Ziu, Coord. Chem. Rev. 216–217 (2001) 513–536.
[26] P.U. Maheswari, V. Rajendiran, R. Parthasarathi, V. Subramanian, M. Palaniandavar, J. Inorg. Biochem. 100 (2006) 3–17;
Y. Nakabayashi, Sens. Actuators, B. 76 (2001) 215.
[27] W.P. Rogers, F.P. Dwyer, E.C. Gyarfas, Aust. J. Biol. Sci. 10 (1957) 342.
[28] K. O′Donoghue, J.C. Penedo, J.M. Kelly, P.E. Kruger, Dalton Trans. (2005) 1123–1128.
[29] T.M. Sielecki, J.F. Boylan, P.A. Benfield, G.L. Trainor, J. Med. Chem. 43 (1999) 1–18.
[30] Z. Zang, L. Jin, X. Qian, M. Wei, Y. Wang, J. Wang, Y. Yang, Q. Xu, Y. Xu, F. Liu, ChemBioChem 8 (2007) 113–121.
[31] P.K.-M. Siu, D.-L. Ma, C.M. Che, Chem. Commun. (2005) 1025–1027.
[32] V.G. Vaidyanathan, B.U. Nair, Eur. J. Inorg. Chem. (2005) 3756–3759.
[33] V. Rajendiran, R. Karthik, M. Palaniandavar, H.S. Evans, V.S. Periasamy, M.A. Akbarsha, B.S. Srinag, H. Krishnamurthy, Inorg. Chem. 46 (2007) 8208–8221.
[34] J. Olofsson, L.M. Wilhelmsson, P. Lincoln, JACS. 126 (2004) 15458–15465.
[35] M.A. Haga, Inorg. Chim. Acta 75 (1983) 29–35.
[36] S. Bhattacharya, Polyhedron 12 (1993) 235.
[37] D.E. Morris, K.W. Hanckand, M.K. Dearmond, Inorg. Chem. 24 (1985) 977.
[38] A.E. Friedman, C.V. Kumar, N.J. Turro, J.K. Barton, Nucleic Acids Res. 19 (1991) 2595–2602.
[39] J.D. McGhee, P.H. von Hippel, J. Mol. Biol. 86 (1974) 469–489.
[40] C. Hiort, B. Norden, A. Rodger, J. Am. Chem. Soc. 112 (1990) 1971–1982.
[41] V.I. Ivanov, L.E. Minchenkova, A.K. Schyolkina, A.I. Poletayer, Biopolymers 12 (1973) 89–110.
[42] B. Norden, F. Tjerneld, Bioploymers 21 (1982) 1713–1734.
[43] J.L. Seifert, R.E. Connor, S.A. Kushon, M. Wang, B.A. Armitage, J. Am. Chem. Soc. 121 (1999) 2987.
[44] L. Messori, P. Orioli, D. Vullo, E. Alessio, E. Lengo, Eur. J. Biochem. 267 (2000) 1206–1213.
[45] V. Rajendiran, M. Palaniandavar, V.S. Periasamy, M.A. Akbarsha, J. Inorg. Biochem. 104 (2010) 217–220.
[46] D. Maniatis, E.F. Fritsch, J. Sambrook, In: Molecular Cloning: A Laboratory Manual, Cold Spring Harbor Laboratory Press, Plainview, NY, 1998, p. 149.
[47] D. Ren, B. Navarro, G. Perez, A.C. Jackson, S. Hsu, Q. Shi, J.L. Tilly, D.E. Clapham, Nature 413 (2004) 603–609.
[48] V.D. Parker, In: in: A.J. Bard (Ed.), Electroanalytical Chemistry, Vol. 14, Marcel Dekker, New York, 1989, p. 18.
[49] M.E. Reichmann, S.A. Rice, C.A. Thomas, P. Poty, J. Am. Chem. Soc. 76 (1954) 3047–3305.
[50] C.M. Dupureur, J.K. Barton, Inorg. Chem. 36 (1997) 33–43.
[51] J.G. Collins, A.D. Sleeman, J.R. Aldrich, I. Greguric, T.W. Hambley, Inorg. Chem. 37 (1998) 3133–3141.
[52] B.P. Sullivan, D.J. Salmon, T.J. Meyer, Inorg. Chem. 17 (1978) 3334–3341.
[53] P.J. Steel, F. Lahousse, D. Lerner, C. Marzin, Inorg. Chem. 22 (1983) 1488–1493.
[54] A.J. Downard, G.E. Honey, P.J. Steel, Inorg. Chem. 30 (1991) 3733–3737.
[55] G. Orellena, C.A. Ibarra, J. Santoro, Inorg. Chem. 27 (1988) 1025–1030.
[56] E.C. Constable, J. Lewis, Inorg. Chim. Acta 70 (1983) 251.
[57] D.P. Segers, M.K. DeArmond, J. Phys. Chem. 86 (1982) 3768.
[58] F.E. Lytle, L.M. Petrosky, L.R. Carlson, Anal. Chim. Acta 57 (1971) 239.
[59] D. Maniatis, E.F. Fritsch, J. Sambrook, Molecular Cloning: A Laboratory Manual, Cold Spring Harbor Laboratory Press, Plainview, NY, 1998. p. 149.
[60] M. Blagosklonny, W.S. El-Diery, Int. J. Cancer 67 (1996) 386–392.